

Short Communication

Synthesis of Metal (Pd, Cu)/Nitrogen doped Asphalt Based Porous Carbon and Its Application for Electrochemical Carbon Dioxide Reduction

Xiaoli Zhu^{1*} and Chusheng Wang²

¹ Institute of Architectural Engineering, Shanghai Zhongqiao Vocational and Technical University, Shanghai 201514, China

² School of Management Science and Engineering, Chongqing Technology and Business University, Chongqing 400067, China

*E-mail: zhuxiaoli40@163.com

Received: 18 August 2022 / Accepted: 15 September 2022 / Published: 10 October 2022

Noble metal-nitrogen co-doped asphalt-based carbon nanocomposites were prepared by introducing noble metal salts using nitrogen-rich asphalt as a precursor and sodium chloride as a template. The effects of noble metal type and doping amount on the catalytic activity of the electrochemical CO₂ reduction reaction of asphalt-based carbon materials were investigated. The electrochemical performance tests showed that the 1% doped nanocomposite catalyst had the best results in 0.5 M of KHCO₃ solution containing saturated CO₂. In addition, the results compared with those of the N₂ solution (starting voltage: -1.75 V, reduction current: -0.5 mA) also indicated that the catalyst effectively inhibits the hydrogen precipitation reaction during CO₂ reduction. Electrochemical impedance tests further validated the results of cyclic voltammetry tests. The results showed that the catalyst had the fastest surface charge migration rate with the highest electrocatalytic activity. CO₂⁻ intermediate plays a key role in CO₂ reduction. HCO₃⁻ is involved in the reaction and has a specific promotion effect on the reaction, and its concentration and reaction rate are positively correlated.

Keywords: CO₂; Asphalt; Catalyst; Nanocomposite; Nitrogen-rich pitch

1. INTRODUCTION

Petroleum asphalt is an important petroleum product with two primary sources: one from natural asphalt ore and one from heavy oil processing such as reduced pressure residual oil, catalytic cracking slurry, and steam cracking tar [1–3]. Typically, petroleum asphalt is a black solid or semi-solid viscous substance. Petroleum asphalt is a colloidal system with asphaltenes as the core to form micelles and dispersed in saturated and aromatic phenols[4], whose molecular structure is dominated by C and H

elements while containing S, N, O, Ni, V, etc. Petroleum asphalt is mainly used in construction and road building, with low industrial added value [5,6]. In recent years, petroleum asphalt as raw material to produce carbon materials, such as petroleum coke, carbon fiber, graphene, activated carbon, etc. Among them, producing high-performance carbon materials from petroleum asphalt has become a new research hotspot and economic growth point [7,8].

The preparation of carbon materials from petroleum asphalt has its natural advantages. Firstly, the carbon content of petroleum asphalt is high, and its mass fraction can reach more than 80%. Secondly, the molecular structure of petroleum asphalt is rich in thick ring aromatic hydrocarbons, which can easily be further condensed under heating conditions to produce carbon predecessors, thus having a high carbon yield [9–11]. Third, the price of petroleum asphalt is low compared to other carbon sources. Petroleum asphalt to carbon material needs to go through a complex reaction process, and the reaction mechanism differs depending on the type of carbon material obtained [12,13]. Generally, it can be divided into 3 stages: thermal condensation, generation of carbon precursors, and high-temperature graphitization [14]. Among the published mechanisms of bitumen carbonization, the theory of the carbonaceous intermediate phase is the most maturely developed and widely applied.

The preparation of petroleum asphalt-based carbon materials is divided into two main categories. The first type is the direct pyrolysis method. The direct pyrolysis method is the most common method for preparing carbon materials in the industry, which is generally performed at higher than 500°C and under inert gas protection [15,16]. The composition and structure of the carbon material obtained by direct pyrolysis are closely related to the feedstock composition, the type of feedstock pretreatment process, and the process conditions [17]. The second type is the template-assisted pyrolysis method [18]. Template-assisted pyrolysis refers to petroleum asphalt pyrolysis mixed with a certain percentage of additives as a template, using additives to regulate the composition and morphology of the resulting carbon material [19]. During the pyrolysis process, the template additive can be added either before or after. The role of template additives is mainly: (1) catalyzing the pyrolysis process of petroleum asphalt and reducing the pyrolysis temperature; (2) promoting and regulating the formation of pore structure in carbon materials and increasing the specific surface area of petroleum asphalt-based carbon materials; (3) heteroatom doping of petroleum asphalt-based carbon materials using the thermal reaction characteristics of the template additive itself, thereby modulating the catalytic properties of the resulting carbon materials [20].

Petroleum asphalt-based carbon materials have a wide range of electrochemical applications. At present, petroleum asphalt-based carbon materials in lithium-ion batteries have been studied more, and many regular understandings have been obtained. Kim et al. [21] systematically investigated the relationship between the softening point of asphalt (100-150°C) and the resulting carbon materials' initial coulombic efficiency and multiplicative properties. They demonstrated that asphalt with a high softening point could yield carbon materials with high crystallinity and thus high multiplicity and initial coulombic efficiency through polymerization and condensation reactions. Petroleum asphalt-based carbon materials for lithium-ion batteries are mainly based on soft carbon, including direct use and encapsulated commercial graphite. However, the key issue that currently restricts its large-scale application is the stability of the raw material source and the fine regulation of the raw material composition. Petroleum pitch-based carbon materials will also be used in sodium battery studies. Wenzel et al. [22] obtained a

porous carbon material by pyrolysis using porous silicon as a template and intermediate phase pitch as a carbon source. This material possesses a capacity of 130 (mA·h)/g, but its initial coulombic efficiency is only 14%. The specific surface area of the carbon material obtained by direct pyrolysis of petroleum asphalt is low and unsuitable for capacitated carbon use. However, after treatment with templating agents and activators, petroleum asphalt can be converted into activated carbon with a large specific surface area. Choi et al. [23] prepared activated carbon using petroleum pitch as the carbon source and assembled it into a double-layer capacitor using charring at 500-1000°C, followed by activation with KOH (900°C).

Since the industrial revolution, over-reliance on fossil fuels has led to a steady rise in atmospheric CO₂ concentrations, which has led to many energy and environmental problems. In order to achieve CO₂ emission reduction and resource utilization, carbon dioxide electro-reduction technology was born [24,25]. This technology uses water as a hydrogen donor and couples electrolytic water reaction with CO₂ hydrogenation reaction to produce chemical raw materials and energy small molecules such as syngas, formic acid, methanol, ethylene, and ethanol. CO₂ is a molecular compound with a highly stable structure. Electrocatalysts are used in it to accelerate the reduction reaction and inhibit the formation of by-products [26]. Electrocatalysts play a decisive role in the activity and product selectivity of the CO₂ reduction reaction, so the study of electrochemical CO₂ reduction electrocatalysts has become a current research hotspot [27]. Carbon-based catalysts have become a current research hotspot due to their low production costs and good stability [28–30]. Quinoline-derived nitrogen-rich pitch has preliminary applications in electrochemistry as a soft carbon source due to its high nitrogen content and solid electrical conductivity. In the study of electrochemical CO₂ reduction electrocatalysts, both high nitrogen content and strong electrical conductivity significantly promote electrocatalyst performance [31]. Therefore, nitrogen-rich asphalt can be applied as a carbon and nitrogen source in electrochemical CO₂ reduction studies. This work investigates the preparation of noble metal/nitrogen-rich asphalt-based carbon catalysts with different metal loadings by sodium borohydride reduction and performs a series of characterization and performance tests for the electrochemical reduction of CO₂.

2. EXPERIMENTAL

2.1. Reagents and instruments

Quinoline was purchased from Shanghai Maclean Biochemical Technology Co. Sodium chloride was purchased from Tianjin Comio Chemical Reagent Co. Palladium chloride was purchased from Beijing Yindu Precious Metals Co. Sodium borohydride was purchased from Guang Dong Guanghua Chemical Factory Co. Copper ethanoate was purchased from Xilong Chemical Co.

2.2. Preparation of nitrogen-rich asphalt

Nitrogen-rich asphalts were prepared by catalytic polycondensation [32], using quinoline as the polymerization monomer, under the catalytic polymerization of an acidic catalyst (AlCl₃). The process was as follows: 1 M of quinoline (C₉H₇N) and 0.5 M of AlCl₃ was quickly weighed in a three-neck flask

and condensed and refluxed under a nitrogen atmosphere at 300°C for 8 h. After the reaction was completed and brought to room temperature, the product was dried in an oven after being washed with acid (HCl solution) and water.

2.3. Preparation of nitrogen-rich asphalt-based porous carbon (NAC)

Add 250 mg of the nitrogen-rich pitch to 15 mL of NMP, dissolve thoroughly and add 2.5 g of sodium chloride. After stirring the solution well using a magnetic stirrer, the solution is brought to 180°C, and the solvent is evaporated. The resulting gray powder is placed in a tube furnace and heated to 900°C in a nitrogen atmosphere at a rate of 5°C/min and maintained for 2 h. After natural reduction to room temperature, the sodium chloride template is removed with a simple water wash to obtain NAC.

2.4. Preparation of NAC-metal nanocomposite

Preparation of Pd/NAC catalysts with different loadings (0.5%, 1%, 3%): Take 3 groups of NAC (0.3 g) and 300 mL of water and sonicate for 2 h. Dissolve 0.0025 g, 0.005 g, and 0.015 g of PdCl₂ in 10 mL of 1:50 dilute hydrochloric acid from 3 groups, stir until the solution is clear, and add to the NAC solution, and stir for 10 min. Add concentrated ammonia drop by drop, adjust pH>10.0, and stir magnetically for 2 h. Take 40 mL of water, adjust pH>10, and put it in an ice water mixture to cool down. Weigh 2 g of sodium borohydride and slowly dissolve it into deionized water at pH=10. Immediately add the sodium borohydride solution drop by drop to the NAC solution under ice bath conditions, adjust the stirring speed after the drop addition and let it react at room temperature for 12 h. After the reaction is complete, wash with plenty of water. The resulting sample was dried in a vacuum oven at 60 °C for 12h. The result products were denoted as Pd/N-AC-05, Pd/N-AC-1 and Pd/N-AC-3 for loading of 0.5%, 1%, 3%, respectively.

Preparation of Cu/NAC catalysts with different loadings (0.5%, 1%, 3%): Take 4 groups of NAC (0.3 g) and 300 mL of water and sonicate for 2 h. Take 4 groups of 10 mL of water and dissolve 0.0047 g, 0.0094 g, and 0.0281 g of copper acetate, stir until the solution is transparent, add to the NAC solution, and stir for 10 min. Add concentrated ammonia drop by drop, adjust pH 10.0, and stir magnetically for 2 h. Take 40 ml of water, adjust pH 10, and put it in an ice water mixture to cool down. Weigh 2 g of sodium borohydride and slowly dissolve it in water at pH=10. Immediately add the sodium borohydride solution drop by drop to the NAC solution under ice bath conditions, adjust the stirring speed after the drop addition and let it react at room temperature for 12 h. After the reaction is complete, wash with plenty of water. The resulting specimens were dried in a vacuum oven at 60°C for 12h. The result products were denoted as Cu/N-AC-05, Cu/N-AC-1 and Cu/N-AC-3 for loading of 0.5%, 1%, 3%, respectively.

2.5. CO₂ electrochemical reduction

The CHI610 model electrochemical workstation (Shanghai Chenhua Instruments Co., Ltd.) and the conventional three-electrode electrochemical apparatus were used to perform the electrochemical reduction performance of CO₂. The working electrode is a catalyst-loaded glassy carbon electrode, the auxiliary electrode is a platinum wire, and the reference electrode is an Ag/AgCl electrode.

The working electrode was prepared by mixing 1.0 mg of catalyst, 50 μ L of 5% Nafion solution and 1 mL of anhydrous ethanol and shaking with ultrasound for 30 min. 10 μ L of the mixture was pipetted onto the surface of the glassy carbon electrode using a microsampler, avoiding spillage of the liquid from the electrode during the operation. The electrode was dried with an infrared lamp to remove the volatile ethanol solvent. Before the experiment, CO₂ (99.99% purity) was added to the electrolyte for 30 min to saturate the gas, and N₂ (99.99% purity) was added to the electrolyte of the blank group for 30 min to eliminate the interference of CO₂ gas in the electrolyte.

In cyclic voltammetric scanning, the potential range of the scan was 0~-2 V, and the scan rate was 400 mV/s. The constant voltage for the timing current test was -1.50 V, the scan rate was 400 mV/s. The constant voltage for the electrochemical impedance test was -1.3 V, the frequency range was 1~10⁵ Hz, and the amplitude of the sinusoidal perturbation potential was 5 mV.

4. RESULTS AND DISCUSSION

NAC is a material prepared using sodium chloride templates, and the templates mainly influence the morphology of the material. Figure 1 shows the morphology of NAC. After the removal of the template by water washing, interconnected mesh-like nanosheet structures were formed in the more concentrated areas of the template due to the occupancy effect of sodium chloride [33]. The sparse areas of the stencil formed the morphology of nanosheet accumulation.

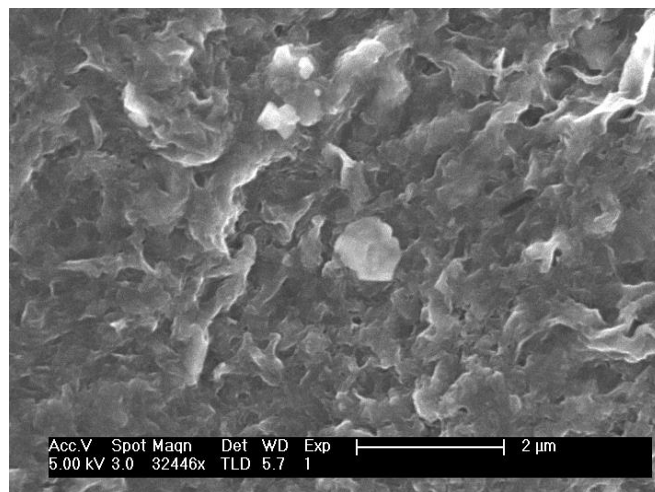


Figure 1. SEM image of nitrogen doped asphalt based porous carbon.

We then performed XRD tests on the NAC. As shown in Figure 2A, the XRD image of NAC showed only the diffraction peaks of carbon, and no other peaks were evident, which proved the high purity of the synthesized NAC. Figure 2B shows the Raman spectrum of NAC, and it can be found that the I_D/I_G value of NAC is 0.979. The higher degree of graphitization allows the carbon material to have a higher electrical conductivity [34]. In addition, the pore structure plays an important role in the catalytic performance and product selectivity. We used N_2 adsorption and desorption isotherms to analyze the pore structure of NAC. The test results are shown in Figure 2C. The BET-specific surface area of NAC is $533 \text{ m}^2/\text{g}$, and the pore volume is $0.27 \text{ cm}^3/\text{g}$. The pore size distribution is shown in Figure 2D. The NAC is a graded porous structure with abundant mesopores and macropores [35]. The rich pore structure is conducive to the complete infiltration of electrolytes, the promotion of electrocatalytic reaction, the adsorption of CO_2 , and the desorption of products [36].

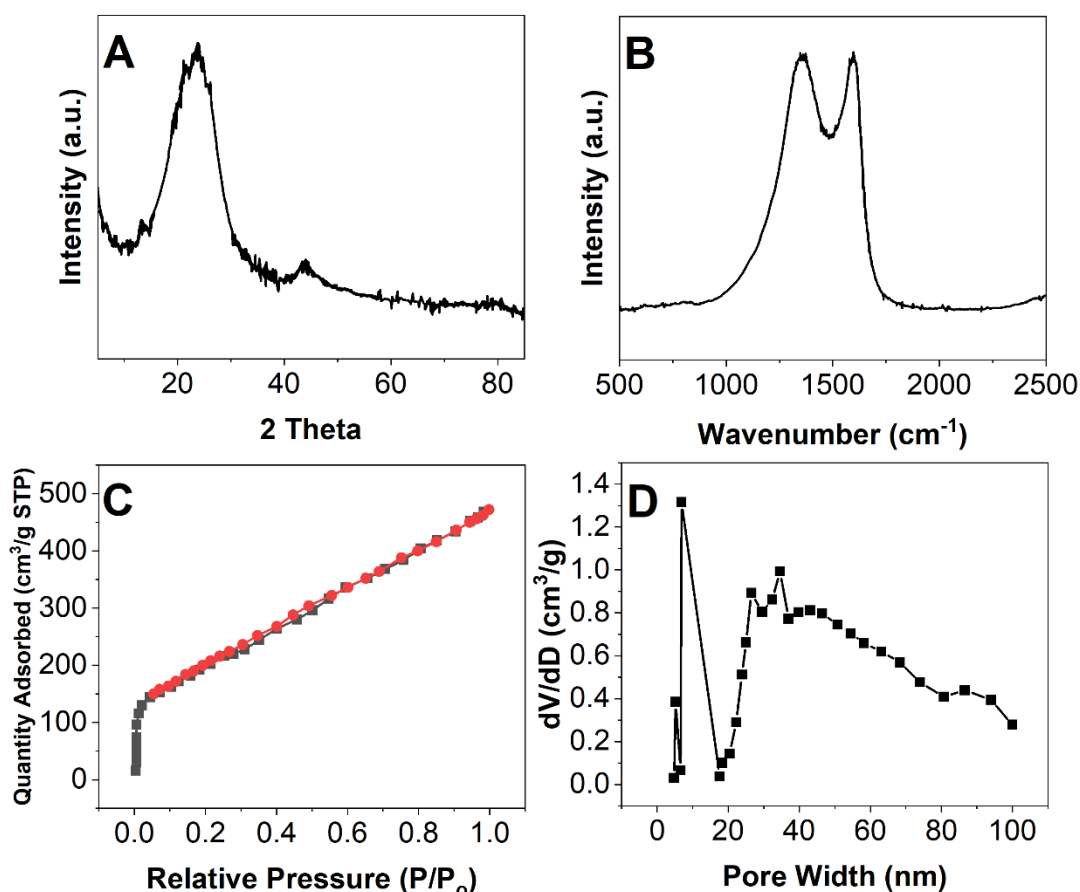


Figure 2. (A) XRD, (B) Raman spectrum, (C) N_2 adsorption and (D) pore size of nitrogen doped asphalt based porous carbon.

Figure 3 shows the XRD characterization results of the NAC-Pd and NAC-Cu catalysts. The very strong diffraction peak observed at 25° in the figure is the characteristic peak of NAC. The characteristic peak of Pd for the Pd/N-AC-05 catalyst appears at 39.8° . The characteristic peaks of Pd for both NAC-Pd-1% and NAC-Pd-3% catalysts appear at 39.7° , known to be the (111) crystal plane of Pd. The XRD

characterization results in Figure 3B show that the diffraction peaks of Cu all appear at 43° , corresponding to the (111) crystal plane of Cu. These characterization results indicate that the metal salts have been successfully reduced to metallic Pd and Cu monomers [37,38]. The diffraction peak corresponding to the (111) crystal plane of Pd is the highest intensity diffraction peak, except for the other crystal planes (111), (200), (220), and (311), where the diffraction peaks are at 40.1° , 46.6° , 68.1° , and 82.1° [39], respectively.

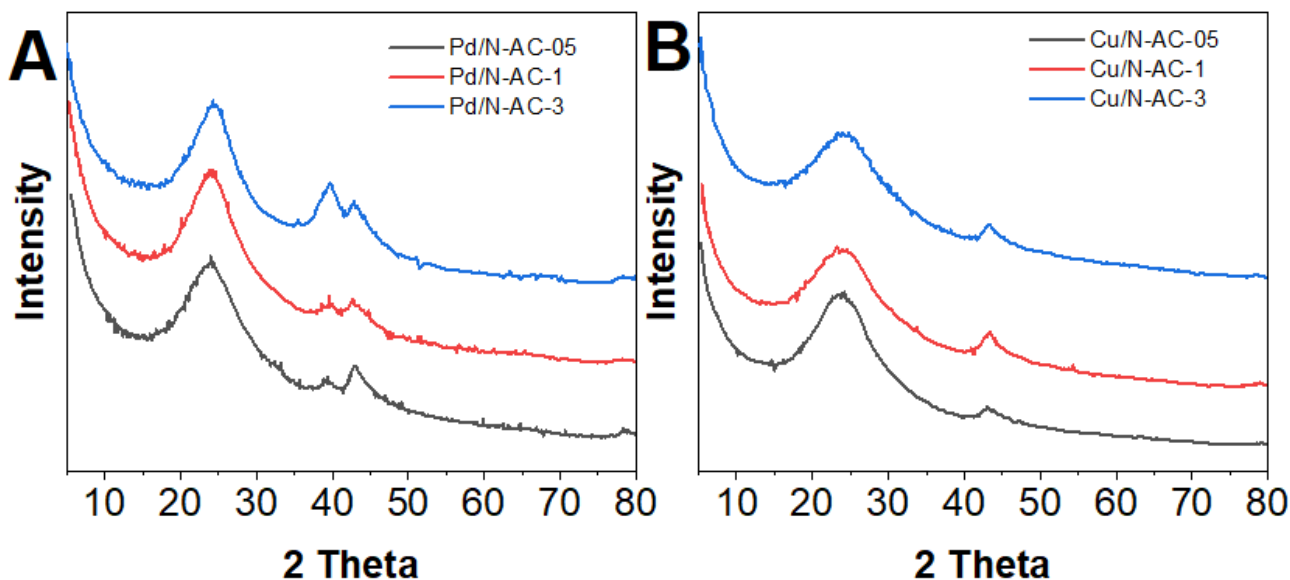


Figure 3. XRD pattern of (A) Pd/N-AC-05, Pd/N-AC-1, Pd/N-AC-3, (B) Cu/N-AC-05, Cu/N-AC-1 and Cu/N-AC-3.

Figure 4 shows the cyclic voltammetric (CV) and the timing current (I-t) for three NAC-Pd catalysts with 0.5%, 1%, and 3% loading in an electrolyte of 0.5 M KHCO_3 . It can be seen that the starting potentials of the reduction currents on the three NAC-Pd catalysts in the electrolyte solution saturated with CO_2 are significantly smaller than those of the blank solution, indicating that different reactions occur on the catalysts [37]. From the figure, it can also be concluded that the value of the reduction current in the electrolyte solution saturated with CO_2 is more significant than that in the blank solution for a specific potential range [40]. The reduction currents on the three catalysts increased with the negative shift of the potential. The Pd/N-AC-1 electrode showed the most significant increase of -1.88 mA, followed by the Pd/N-AC-05 electrode, and the Pd/N-AC-3 electrode showed the smallest increase. The reduction currents of both reached -1.42 mA and -0.30 mA, respectively. In contrast, the reduction current on the catalyst surface in the blank solution was negligible [41]. This indicates that the CO_2 reduction on the Pd/N-AC-1 catalyst is higher when the reduction potential is more negative. In the N_2 -saturated atmosphere, hydrogen precipitation reaction mainly occurs on the catalyst surface. In addition to the hydrogen precipitation reaction. The reduction reaction of CO_2 also occurs in the CO_2 -saturated electrolyte solution, so the reduction current will differ [42]. The I-t diagram in the figure shows that the current decays relatively fast in the first 5 s for each catalyst. After that, the decay rate of the current with time decreases significantly for all catalysts. Compared to the decay rate of the current

in the CO₂ atmosphere and the reduction current, the decay rate of the current in the N₂ solution and its value is significantly smaller. Therefore, it can be indicated that CO₂ exhibits a more stable catalytic performance when reacting on the catalyst surface [38].

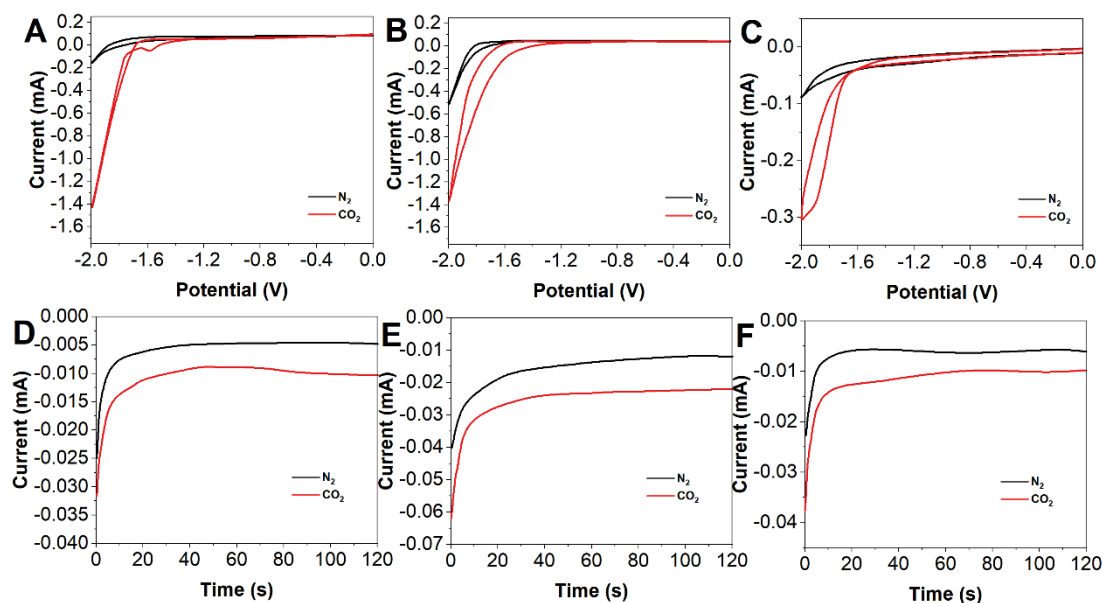


Figure 4. CVs of (A) Pd/N-AC-05, (B) Pd/N-AC-1, (C) Pd/N-AC-3 of CO₂ reduction. Chronoamperometry curves of (D) Pd/N-AC-05, (E) Pd/N-AC-1, (F) Pd/N-AC-3 in CO₂-saturated 0.5 M KHCO₃.

Figure 5 shows the CV and I-t for three NAC-Cu catalysts with 0.5%, 1%, and 3% loading in an electrolyte of 0.5 M KHCO₃. The CV results in Figure 5 show that the reduction currents' starting potentials on the three NAC-Cu catalysts are significantly smaller than those of the blank solution in the CO₂-saturated electrolyte solution [43]. Among them, the starting voltage of the Cu/N-AC-1 catalyst is -1.3 V. The starting voltage of NAC-Cu for the other 2 loading amounts is -1.4 V, while the starting voltage under the N₂ atmosphere is -1.75 V. This indicates a different reaction over the catalyst due to the more positive reduction potential of CO₂. This indicates that the catalyst under the CO₂ atmosphere preferentially undergoes a reduction-oriented reaction. In addition, the reduction current in the electrolyte solution under a CO₂ atmosphere is larger than that in the blank solution for a certain potential range [44]. Cu/N-AC-1 produced a maximum reduction current value as high as -2.25 mA, much larger than the reduction current produced by each catalyst in the N₂ solution. This is due to hydrogen precipitation processes on the catalyst surface in N₂-saturated solutions [45]. In addition to the hydrogen precipitation reaction, electrochemical reduction of CO₂ occurs in CO₂-saturated electrolyte solutions [46]. From the I-t curve, it can be seen that the current decays faster in the first 10 s for all three catalysts in both solutions. After that, the decay rate of the current with time decreases significantly on each catalyst [47]. The decay rate of the reduction current generated by each catalyst is lower in CO₂ than in the N₂ atmosphere. This indicates that all three NAC-Cu catalysts have an obvious catalytic effect on

CO₂ and the catalytic performance is relatively stable. The performance of the proposed catalyst is comparable to those of previously reported catalysts for CO₂ reduction (Table 1).

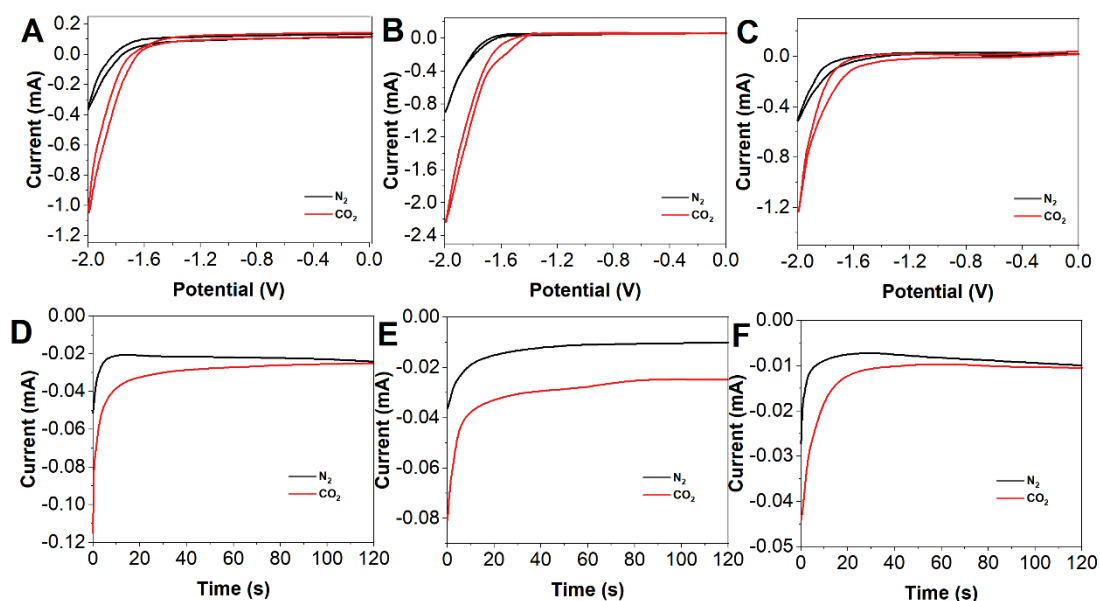


Figure 5. CVs of (A) Cu/N-AC-05, (B) Cu/N-AC-1, (C) Cu/N-AC-3 of CO₂ reduction. Chronoamperometry curves of (D) Cu/N-AC-05, (E) Cu/N-AC-1, (F) Cu/N-AC-3 in CO₂-saturated 0.5 M KHCO₃.

Figure 6 shows the EIS plots of NAC-Pd-1% and Cu/N-AC-1 in saturated CO₂ with 0.5 M KHCO₃. As shown in Figure 6, the electrochemical impedance spectra of the 2 catalysts showed a similar semicircular shape, which indicated that the reaction of electrochemical reduction of CO₂ was mainly controlled by charge migration [48]. Among them, the decrease in the radius of the impedance arc indicates a faster rate of charge migration on the catalyst surface, which enhances the CO₂ reduction efficiency [49]. The test results show that the charge migration on the surface of the Cu/N-AC-1 catalyst is faster with a higher electrocatalytic activity [50,51]. The test results show that the Cu/N-AC-1 catalyst has a faster charge migration on the surface, representing excellent electrocatalytic activity.

Table 1. Comparison of performances of NAC-Pd with previous reports for CO₂ reduction.

Catalyst	Potential (V)	J (mA/cm ²)	Ref
c-Cu ₂ O	-1.4	~14	[52]
Cu ₂ O/NRGO	-1.4	~12	[53]
Au _{0.02} Cu ₂ O	-1.3	~5.7	[54]
Cu/N-AC-1	-1.3	~7	This work

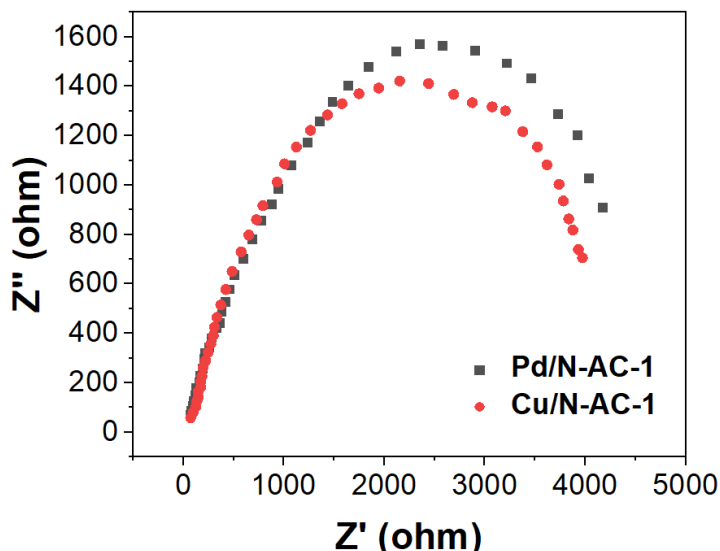


Figure 6. EIS plots of Pd/N-AC-1 and Cu/N-AC-1 in CO₂-saturated KHCO₃.

4. CONCLUSION

This work uses nitrogen-rich asphalt as a nitrogen and nitrogen source and sodium chloride as a template to form nanocomposite catalysts by introducing nano-palladium and nano-copper. The morphology and structure of the synthesized materials were characterized using SEM, Raman, XRD, and N₂ adsorption. We also examined the catalytic activity of different catalysts in the electrochemical CO₂ reduction reaction. In CO₂-saturated electrolyte solutions, the starting potentials of each catalyst surface when generating reduction currents were significantly smaller than those of blank solutions, indicating that different reactions occurred at the catalyst surfaces. Since the reduction potential in the CO₂-saturated electrolyte solution is more optimistic, it indicates that the CO₂ reduction-based reaction occurs preferentially on the catalyst surface. The reduction current was significantly more extensive than that of the blank solution when the hydrogen precipitation reaction occurred. Among the monometallic NAC catalysts, Pd/N-AC-1 and Cu/N-AC-1 catalysts showed better catalytic effects with the starting potential of -1.3 V and reduction currents of -1.88 mA -2.25 mA, respectively.

ACKNOWLEDGEMENTS

This work was supported by Key project of "Fourteenth Five-year Plan" of Chongqing Education Science "BIM based Project Management Professional Knowledge Fragmentation and Systematic Ability Connection Approach" (Project Number: 2021-GX-125).

References

1. L. Pan, X. Li, Y. Wang, J. Liu, W. Tian, H. Ning, M. Wu, *Applied Surface Science*, 444 (2018) 739–746.

2. L. Pan, Y. Wang, H. Hu, X. Li, J. Liu, L. Guan, W. Tian, X. Wang, Y. Li, M. Wu, *Carbon*, 134 (2018) 345–353.
3. Y. Zhu, Y. Wang, C. Gao, W. Zhao, X. Wang, M. Wu, *New Carbon Materials*, 35 (2020) 358–370.
4. H. Karimi-Maleh, C. Karaman, O. Karaman, F. Karimi, Y. Vasseghian, L. Fu, M. Baghayeri, J. Rouhi, P. Senthil Kumar, P.-L. Show, S. Rajendran, A.L. Sanati, A. Mirabi, *Journal of Nanostructure in Chemistry*, 12 (2022) 429–439.
5. Y. Ding, B. Shan, X. Cao, Y. Liu, M. Huang, B. Tang, *Journal of Cleaner Production*, 288 (2021) 125586.
6. G.D. da Silveira, L.M. de Carvalho, N. Montoya, A. Domenech-Carbó, *Electrochimica Acta*, 270 (2018) 461–470.
7. F. Rovasi Adolfo, P. Cícero do Nascimento, D. Bohrer, C. Viana, L. Machado de Carvalho, M.C. Coutinho Cravo, L. Nascimento, *Fuel*, 277 (2020) 118098.
8. J. Liu, Y. Liu, P. Li, L. Wang, H. Zhang, H. Liu, J. Liu, Y. Wang, W. Tian, X. Wang, Z. Li, M. Wu, *Carbon*, 126 (2018) 1–8.
9. Y. Li, W. Yang, Z. Tu, S. Che, C. Xu, H. Liu, G. Huang, Y. Li, *Carbon*, 182 (2021) 700–710.
10. W. Zhang, L. Qiu, J. Liu, K. Hu, L. Zou, Y. Chen, C. Yang, F. Wang, J. Zang, *Construction and Building Materials*, 306 (2021) 124740.
11. J. Li, F. Zhang, Y. Liu, Y. Muhammad, Z. Su, F. Meng, X. Chen, *Construction and Building Materials*, 201 (2019) 268–277.
12. W. Yang, R. Li, B. Jiang, T. Wang, L. Hou, Z. Li, Z. Liu, F. Yang, Y. Li, *Carbon*, 166 (2020) 218–226.
13. Q. Zhao, X. Tan, T. Ma, F. Cao, Z. Xia, H. Liu, H. Ning, Z. Li, H. Hu, M. Wu, *Journal of Colloid and Interface Science*, 587 (2021) 810–819.
14. W. Yang, B. Deng, L. Hou, T. Wang, J. Tian, S. Wang, R. Li, F. Yang, Y. Li, *Chemical Engineering Journal*, 380 (2020) 122552.
15. A.M. Al-Sabaei, M.B. Napiyah, M.H. Sutanto, W.S. Alaloul, A. Usman, *Journal of Cleaner Production*, 249 (2020) 119357.
16. J. Shi, P. Zhao, W. Fan, Z. Yang, Y. Lin, J. Ouyang, *Construction and Building Materials*, 262 (2020) 120073.
17. B. Li, B. Wang, X. Zhang, X. Lin, Y. Zhang, *Advances in Materials Science and Engineering*, 2022 (2022) 4901879.
18. H. Karimi-Maleh, M. Alizadeh, Y. Orooji, F. Karimi, M. Baghayeri, J. Rouhi, S. Tajik, H. Beitollahi, S. Agarwal, V.K. Gupta, S. Rajendran, S. Rostammia, L. Fu, F. Saberi-Movahed, S. Malekmohammadi, *Ind. Eng. Chem. Res.*, 60 (2021) 816–823.
19. H. Karimi-Maleh, A. Ayati, R. Davoodi, B. Tanhaei, F. Karimi, S. Malekmohammadi, Y. Orooji, L. Fu, M. Sillanpää, *Journal of Cleaner Production*, 291 (2021) 125880.
20. Q. Wang, *Advances in Materials Science and Engineering*, 2022 (2022) 4636049.
21. B.-H. Kim, J.-H. Kim, J.-G. Kim, J.S. Im, C.W. Lee, S. Kim, *Journal of Industrial and Engineering Chemistry*, 45 (2017) 99–104.
22. S. Wenzel, T. Hara, J. Janek, P. Adelhelm, *Energy & Environmental Science*, 4 (2011) 3342–3345.
23. D. Kim, J. Cheon, J. Kim, D. Hwang, I. Hong, O.H. Kwon, W.H. Park, D. Cho, *Carbon Letters*, 22 (2017) 81–88.
24. H. Zhang, J. Li, S. Xi, Y. Du, X. Hai, J. Wang, H. Xu, G. Wu, J. Zhang, J. Lu, *Angewandte Chemie*, 131 (2019) 15013–15018.
25. R. Küngas, *Journal of The Electrochemical Society*, 167 (2020) 044508.
26. M.G. Kibria, J.P. Edwards, C.M. Gabardo, C. Dinh, A. Seifitokaldani, D. Sinton, E.H. Sargent, *Advanced Materials*, 31 (2019) 1807166.
27. G.L. De Gregorio, T. Burdyny, A. Loiudice, P. Iyengar, W.A. Smith, R. Buonsanti, *ACS Catalysis*, 10 (2020) 4854–4862.

28. C. Choi, S. Kwon, T. Cheng, M. Xu, P. Tieu, C. Lee, J. Cai, H.M. Lee, X. Pan, X. Duan, *Nature Catalysis*, 3 (2020) 804–812.
29. N. Han, P. Ding, L. He, Y. Li, Y. Li, *Advanced Energy Materials*, 10 (2020) 1902338.
30. S. Xu, E.A. Carter, *Chemical Reviews*, 119 (2018) 6631–6669.
31. T.N. Nguyen, M. Salehi, Q.V. Le, A. Seifitokaldani, C.T. Dinh, *ACS Catalysis*, 10 (2020) 10068–10095.
32. A. Jänes, H. Kurig, E. Lust, *Carbon*, 45 (2007) 1226–1233.
33. M. Zahoor, S. Nizamuddin, S. Madapusi, F. Giustozzi, *Process Safety and Environmental Protection*, 147 (2021) 1135–1159.
34. S. Arafat, N. Kumar, N.M. Wasiuddin, E.O. Owhe, J.G. Lynam, *Journal of Cleaner Production*, 217 (2019) 456–468.
35. R. Zhang, Q. Dai, Z. You, H. Wang, C. Peng, *Applied Sciences*, 8 (2018) 1665.
36. X. Qu, Q. Liu, C. Wang, D. Wang, M. Oeser, *Materials*, 11 (2018) 244.
37. Z. Sadeghtabaghi, A.R. Rabbani, A. Hemmati-Sarapardeh, *Journal of Molecular Structure*, 1238 (2021) 130425.
38. G.S. Reddy, A. Ramesh, V.V. Ramayya, *International Journal of Pavement Research and Technology* (2022).
39. Q. Zeng, Y. Liu, Q. Liu, P. Liu, Y. He, Y. Zeng, *Construction and Building Materials*, 238 (2020) 117706.
40. P. Yaashikaa, P.S. Kumar, S.J. Varjani, A. Saravanan, *Journal of CO2 Utilization*, 33 (2019) 131–147.
41. Y. Katayama, F. Nattino, L. Giordano, J. Hwang, R.R. Rao, O. Andreussi, N. Marzari, Y. Shao-Horn, *The Journal of Physical Chemistry C*, 123 (2018) 5951–5963.
42. K. Fan, Y. Jia, Y. Ji, P. Kuang, B. Zhu, X. Liu, J. Yu, *ACS Catalysis*, 10 (2019) 358–364.
43. T. He, L. Zhang, G. Kour, A. Du, *Journal of CO2 Utilization*, 37 (2020) 272–277.
44. M. Moura de Salles Pupo, R. Kortlever, *ChemPhysChem*, 20 (2019) 2926–2935.
45. Y. Zhou, R. Zhou, X. Zhu, N. Han, B. Song, T. Liu, G. Hu, Y. Li, J. Lu, Y. Li, *Advanced Materials*, 32 (2020) 2000992.
46. E.M. Nichols, J.S. Derrick, S.K. Nistanaki, P.T. Smith, C.J. Chang, *Chemical Science*, 9 (2018) 2952–2960.
47. Y. Liu, H. Yang, X. Fan, B. Shan, T.J. Meyer, *Chinese Chemical Letters*, 33 (2022) 4691–4694.
48. W. Ong, L.K. Putri, A.R. Mohamed, *Chemistry—A European Journal*, 26 (2020) 9710–9748.
49. F. Franco, C. Rettenmaier, H.S. Jeon, B.R. Cuenya, *Chemical Society Reviews*, 49 (2020) 6884–6946.
50. Y. Zheng, A. Vasileff, X. Zhou, Y. Jiao, M. Jaroniec, S.-Z. Qiao, *Journal of the American Chemical Society*, 141 (2019) 7646–7659.
51. Z. Chen, T. Fan, Y.-Q. Zhang, J. Xiao, M. Gao, N. Duan, J. Zhang, J. Li, Q. Liu, X. Yi, *Applied Catalysis B: Environmental*, 261 (2020) 118243.
52. H. Ning, Q. Mao, W. Wang, Z. Yang, X. Wang, Q. Zhao, Y. Song, M. Wu, *Journal of Alloys and Compounds*, 785 (2019) 7–12.
53. J. Zhang, Y. Guo, B. Shang, T. Fan, X. Lian, P. Huang, Y. Dong, Z. Chen, X. Yi, *ChemSusChem*, 14 (2021) 929–937.
54. X. Cao, G. Cao, M. Li, X. Zhu, J. Han, Q. Ge, H. Wang, *European Journal of Inorganic Chemistry*, 2021 (2021) 2353–2364.